RSC Advances

PAPER

View Article Online
View Journal | View Issue

Cite this: *RSC Adv.*, 2023, **13**, 11002

Facile preparation and dielectric properties of $BaTiO_3$ with different particle sizes and morphologies

Xinxiao Wu, [a] Hepan Zhao,[a] Weining Han,[a] Zhimiao Wang, [a] Fang Li,[ab] Jing Li*[c] and Wei Xue *[ab]

$BaTiO_3$ nanoparticles were prepared by the hydrothermal method, and the effect of 1-(propyl-3-methoxysilyl)-3-methylimidazole chloride on the size of $BaTiO_3$ particles was investigated. The obtained $BaTiO_3$ was characterized by XRD, SEM, TEM, and Raman spectroscopy; and the dielectric properties of $BaTiO_3$ ceramic sheets were tested. The results indicate that the spherical $BaTiO_3$-N prepared without an ionic liquid was in a tetragonal phase with an average particle size of 129 nm. When an ionic liquid was added, the size of the $BaTiO_3$-IL decreased and the degree of agglomeration increased. In addition, with increasing quantity of ionic liquid, the tetragonal-phase content of $BaTiO_3$-IL gradually decreased until complete transformation into cubic phase. The dielectric constant of the $BaTiO_3$-N ceramics was the highest, and the dielectric constant decreased with decreasing $BaTiO_3$ particle size. Moreover, two types of $BaTiO_3$ nanoparticles (bowl- and sea urchin-shaped) were prepared by changing the hydrothermal conditions and additives. The average particle size of the former was 92 nm, the tetragonal-phase content was *ca.* 90%, and the dielectric constant was large; whereas the sea urchin-shaped $BaTiO_3$ consisted of small particles in the cubic phase, and the dielectric constant was small.

Received 31st December 2022
Accepted 2nd April 2023

DOI: 10.1039/d2ra08334e

rsc.li/rsc-advances

1. Introduction

Barium titanate ($BaTiO_3$) is a ferroelectric compound with excellent properties in the barium oxide–titanium dioxide ($BaO–TiO_2$) system,[1] which exhibits good dielectric as well as ferroelectric properties and is the basic material for electronic ceramic components.[2,3] Barium titanate nanoparticles are widely used to make small, high-capacity microcapacitors and temperature-compensating components;[4,5] as well as nonlinear components, dielectric amplifiers, memory components for electronic computers, ceramic sensitive components, microwave ceramics, and piezoelectric ceramics.[6,7] In recent years, with the continuous development of the electronics industry, the demand for $BaTiO_3$-based ceramics has been increasing; and higher requirements for $BaTiO_3$ purity, particle size, crystal shape, and dispersion have been proposed.[1,8] There is broad utility in preparing high-purity, ultrafine $BaTiO_3$ powder.[9,10]

Currently, the main methods for synthesizing nano-$BaTiO_3$ include solid-phase synthesis, co-precipitation, sol–gel, and hydrothermal synthesis.[11,12] Solid-phase synthesis requires a high temperature of *ca.* 1100 °C, and the resulting barium titanate powder exhibits a large grain size as well as low powder purity.[13] Co-precipitation requires high-temperature roasting, which is prone to impart agglomeration of and a nonuniform particle size to the synthesized powder.[12] Sol–gel method process conditions are not suitable for control and the organic solvent is highly toxic.[14,15] In contrast, the hydrothermal method is excellent for preparing $BaTiO_3$ powder.[1] The resulting powder or nanocrystals are well-developed, with a composition close to stoichiometry as well as a uniform and controllable particle size distribution, and the average grain size of the resulting nano-$BaTiO_3$ is small (as little as tens or even several nanometers).[16,17] At present, $BaTiO_3$ particles obtained by hydrothermal preparation with $Ba(OH)_2 \cdot 8H_2O$ and TiO_2 as raw materials are is generally >100 nm in size and require high-temperature calcination to obtain smaller particles.[17,18] Therefore, how to reduce the average size of nano-$BaTiO_3$ particles by hydrothermal synthesis under mild conditions is an active area of research.

Furthermore, the properties of nanomaterials are not only dependent on their size, but the influence of the microscopic morphology is also crucial, which has led to substantial interest in preparing barium titanate in various morphologies and sizes. Ma *et al.*[19] used oleic acid and *tert*-butylamine as additives to synthesize $BaTiO_3$ nanocubes, with a smooth surface and an average size of 25 nm, by the hydrothermal method. Inada *et al.*[20] obtained tetragonal-phase barium titanate nanorods using $BaCl_2$ and $TiCl_4$ as raw materials, and ethylene glycol as

[a]*Hebei Provincial Key Laboratory of Green Chemical Technology, High Efficient Energy Saving, School of Chemical Engineering and Technology, Hebei University of Technology, Tianjin 300130, China. E-mail: weixue@hebut.edu,cn*

[b]*Tianjin Key Laboratory of Chemical Process Safety, Tianjin 300130, China*

[c]*School of Civil and Transportation Engineering, Hebei University of Technology, Tianjin 300401, China*

the solvent by the hydro/solvothermal method. Their mechanistic analysis suggests that ethylene glycol played an important role in the nucleation and anisotropic growth of tetragonal barium titanate. Li *et al.*[21] prepared a nano-$BaTiO_3$ supercage structure—without organic additives—that exhibited excellent microwave absorption. Zhu *et al.*[22] used a simple method to prepare cubic-phase $BaTiO_3$ nanotubes with an average diameter of 10 nm and a wall thickness of 3 nm. The material exhibited excellent high-frequency absorption and is a promising microwave-absorbing material. Surmenev *et al.*[23] prepared one-dimensional, nano/micron-sized, rod-shaped $BaTiO_3$ by the hydrothermal method and found that $BaTiO_3$ with various morphologies, sizes, and phase compositions could be prepared by adjusting the temperature, time, and alkalinity of the hydrothermal process.

Ionic liquids have many unique properties—such as wide electrochemical windows, low surface tension, and high thermal stability.[26,27] In recent years, the advantages of ionic liquids in synthesizing inorganic nanomaterials have been gradually discovered and there are an increasing number of applications.[24,25] Ionic liquids can act as reactants, solvents, and templates in preparing inorganic nanomaterials.[29,30] The low surface tension of ionic liquids can lead to high nucleation rates and Ostwald ripening, and ultimately to small particles. Ionic liquids can also interact with the particle surface and thus play an important role in particle growth.[28] Zhou *et al.*[31] used the ionic liquid [Bmim]BF_4 as an additive and prepared TiO_2 nanocrystals with an average size of only 2–3 nm under mild conditions. Cao *et al.*[32] synthesized ultrafine amorphous metal hydroxide nanoparticles for efficient oxygen evolution by a one-step method with 1-aminopropyl-3-methylimidazolium tetrafluoroborate, resulting in particle sizes of 2–3 nm. Paszkiewicz *et al.*[33] prepared TiO_2 microspheres with ionic liquids as additives. The effect of the cation chain length of imidazole-based ionic liquids on the resulting TiO_2 morphology and photoactivity were systematically studied; both the electrostatic stability and coordination of imidazole cations facilitated growth of TiO_2 spheres. Kim *et al.*[34] prepared Ag nanostructures with various morphologies—including nanowires—with 1-butyl-3-methylimidazole-based ionic liquids as additives, and concluded that forming these morphologies was related to the stabilizing effect as well as self-organization of the ionic liquids.

As mentioned previously, ionic liquids play an important role in preparing inorganic nanomaterials. However, preparing $BaTiO_3$ with ionic liquids has not been reported to date. In the present paper, the 1-(propyl-3-methoxysilyl)-3-methylimidazole chloride ([Tmospmim]Cl) was used as an additive, and anatase TiO_2 as well as $Ba(OH)_2 \cdot 8H_2O$ were used as raw materials to prepare nano-$BaTiO_3$ by the hydrothermal method. The effects of the quantity of ionic liquid on the size, morphology, and tetragonal-phase content of $BaTiO_3$ were investigated; and the dielectric properties of $BaTiO_3$ were measured. In addition, hollow, bowl-shaped nano-$BaTiO_3$ with a small size and excellent dielectric properties was also prepared with polyvinylpyrrolidone (PVP) instead of an ionic liquid.

2. Experimental

2.1 Materials and reagents

$Ba(OH)_2 \cdot 8H_2O$, TiO_2, Polyvinylpyrrolidone (PVP) and ammonia ($NH_3 \cdot H_2O$) were of analytical grade and used without further purification. 1-(Propyl-3-methoxysilyl)-3-methylimidazole chloride ([Tmospmim]Cl, 99%) was purchased from Shanghai Chengjie Chemical Co., Ltd Formic acid anhydrous (HCOOH, 98%) was purchased from Tianjin Comio Chemical Reagent Co., Ltd.

2.2 Hydrothermal synthesis of $BaTiO_3$

Hydrothermal synthesis of $BaTiO_3$ was conducted in a 100 mL PTFE-lined crystallization kettle. Firstly, $Ba(OH)_2 \cdot 8H_2O$ (14.2 g, 45 mmol), TiO_2 (1.4 g, 18 mmol), deionized water (30 mL) and [Tmospmim]Cl (1.0 g, 3.0 g or 5.0 g) were added to the kettle in turn and stirred well. Then, $NH_3 \cdot H_2O$ (14 mL, 25%) was added to adjust the alkalinity of the system. The hydrothermal process was conducted at 200 °C for 48 h. When the reaction was finished, the crystallization kettle was cooled to room temperature and the solid was separated from the liquid. Afterwards, it was repeatedly washed with formic acid (1 mol L^{-1}) and water until the filtrate was neutral. The resulting solid was dried at 80 °C to a constant weight and designated as $BaTiO_3$-IL-X ($X = 1$, 3, or 5).

The preparation process without the addition of ionic liquid was the same as the above steps, and the resulting product was noted as $BaTiO_3$-N.

Urchin-like nano-$BaTiO_3$: $Ba(OH)_2 \cdot 8H_2O$ (4.7 g, 15 mmol), deionized water (30 mL), TiO_2 (0.48 g, 6 mmol) and [Tmospmim]Cl (5.0 g) were added to a 100 mL PTFE-lined crystallization kettle and stirred well. Then, $NH_3 \cdot H_2O$ (25%, 14 mL) was added to adjust the alkalinity. The next reaction procedure was the same as $BaTiO_3$-IL. The prepared urchin-like nano-$BaTiO_3$ was denoted as $BaTiO_3$-U.

Hollow bowl-shaped of nano-$BaTiO_3$: the preparation process was similar to $BaTiO_3$-IL, except that polyvinylpyrrolidone (5.0 g, PVP) was used instead of ionic liquid and the resulting hollow bowl-shaped nano-$BaTiO_3$ was noted as $BaTiO_3$-B.

2.3 Characterization

X-ray diffraction (XRD) of samples were collected with a Bruker D8 Discover X-ray diffractometer using a graphite monochrome filter and Cu Kα radiation. The tube voltage and the tube current were set at 40 kV and 40 mA, respectively. The samples were scanned in the 2θ range of 15–90°, scanning speed of 6° min^{-1}.

Transmission electron microscope (TEM) from FEI Talos F200S with a voltage of 200 kV and a resolution of 0.12 nm was used to observe the morphology and size of $BaTiO_3$ particles.

Scanning electron microscopy (SEM) from the FEI Nova Nano S450 was used to observe the morphology and particle size of the samples by collecting signals from secondary electrons and backscattered electrons for microscopic morphology analysis.

A LabRAM HR Evolution laser Raman spectrometer from HORIBA Jobin Yvon was used to perform the samples with a 532 nm Nd: YAG laser. The spectral range was 100–1000 cm^{-1}, and the spectral resolution was less than 1 cm^{-1}.

Bulk density was measured *via* Archimede's method.

2.4 Electrical performance test

A high frequency dielectric spectrometer, Agilent E4991A, was used to test the dielectric constants and dielectric losses of the ceramic samples at different temperatures at 1000 Hz and a DC voltage of 1 V. The dielectric constants of the $BaTiO_3$ ceramics were calculated according to eqn (1).

$$\varepsilon = C \cdot h / \varepsilon_0 S \quad (1)$$

where: ε_0-vacuum dielectric constant, $\varepsilon_0 = 8.854 \times 10^{-12}$ F m^{-1}, C-type capacitance, F; h-thickness of ceramic sheet, m; S-electrode area, m^2.

The dielectric properties of nano-$BaTiO_3$ with different grain sizes were tested. Paraffin wax of 7% was mixed with 0.8 g nano-$BaTiO_3$ powder, and the wax was fried on a microwave induction oven to make the wax uniformly dispersed in the $BaTiO_3$ powder. The powder was passed through an 80 mesh sieve, sieved, and then pressed into shape under a pressure of 4 MPa to obtain raw flakes.

The raw $BaTiO_3$ ceramic flakes obtained after pressing were placed in a high-temperature sintering furnace for sintering. The sintering procedure is set at room temperature to 550 °C with a heating rate of 2.5 °C min^{-1}. After 550 °C, the binder is removed from the billets by holding them for 1 h. Afterwards, the temperature is rapidly increased to 1250 °C (8 °C min^{-1}) and held for 4 h. After the sintering is completed, the temperature is cooled down (3 °C min^{-1}) to room temperature. Finally, the $BaTiO_3$ ceramic sheets were coated with silver paste on both sides and tested for their dielectric properties after silver firing.

3. Results and discussion

3.1 Preparation of $BaTiO_3$ with various particle sizes

$BaTiO_3$ nanoparticles were prepared by the hydrothermal method with the ionic liquid [Tmospmim]Cl as an additive, and the effect of the quantity of ionic liquid was investigated. The obtained $BaTiO_3$ was characterized (Fig. 1–3).

Fig. 1 shows the XRD patterns of the $BaTiO_3$ samples. Based on the XRD pattern of $BaTiO_3$-N in Fig. 1A, diffraction peaks with 2θ of 22.26°, 31.56°, 38.91°, 45.08°, 45.38°, 51.08°, 56.25°, and 65.78° were evident; corresponding to the (100), (110), (111), (002), (200), (210), (211) and (220) crystal planes, respectively.[35] In particular, the diffraction peak near 45° was split into two peaks (Fig. 1B), which indicates that the prepared $BaTiO_3$-N was in the tetragonal phase (JCPDS NO. 05-0626).[36,47] The calculated axial ratio c/a was 1.0086, which indicates that the content of tetragonal-phase $BaTiO_3$ was approximately 95%.[37] The XRD pattern of $BaTiO_3$-IL was similar to that of $BaTiO_3$-N after adding the ionic liquid [Tmospmim]Cl. However, the split two peaks at 45° gradually merged into a single peak with increasing ionic liquid dosage, indicating that the ionic liquid facilitated formation of the cubic-phase $BaTiO_3$ (JCPDS NO. 31-0174).[38]

Fig. 2 shows the Raman spectra of $BaTiO_3$-N and $BaTiO_3$-IL-5. The Raman peaks of tetragonal $BaTiO_3$ were evident at 185, 260, 307, 515, and 715 cm^{-1} in the spectrum of $BaTiO_3$-N. In contrast, the Raman spectrum of $BaTiO_3$-IL-5 exhibited no peaks, indicating that it exhibited no Raman activity and was all cubic-phase $BaTiO_3$, which is consistent with the XRD results. Adding an ionic liquid facilitated formation of cubic-phase $BaTiO_3$.

Fig. 3 shows SEM and TEM images of $BaTiO_3$ samples, as well as the particle size distributions. As evident from Fig. 3A1 and B1, the $BaTiO_3$-N particles were nearly spherical with uniform size and good dispersion. The diameter of the $BaTiO_3$-N particles was 129 nm. The $BaTiO_3$-IL-1 particles prepared with an ionic liquid were smaller: 86 nm (Fig. 3A2, B2, C2). With increasing quantity of ionic liquid, the particle size of $BaTiO_3$-IL-3 decreased substantially to only 46 nm. However, the dispersion deteriorated with obvious agglomeration. The average particle size of $BaTiO_3$-IL-5 was 34 nm and agglomeration of the particles was substantial. Adding an ionic liquid reduced the surface tension of the system and increased the nucleation rate of $BaTiO_3$, resulting in smaller particles.[28,39] In addition, the viscosity of the reaction system increases with

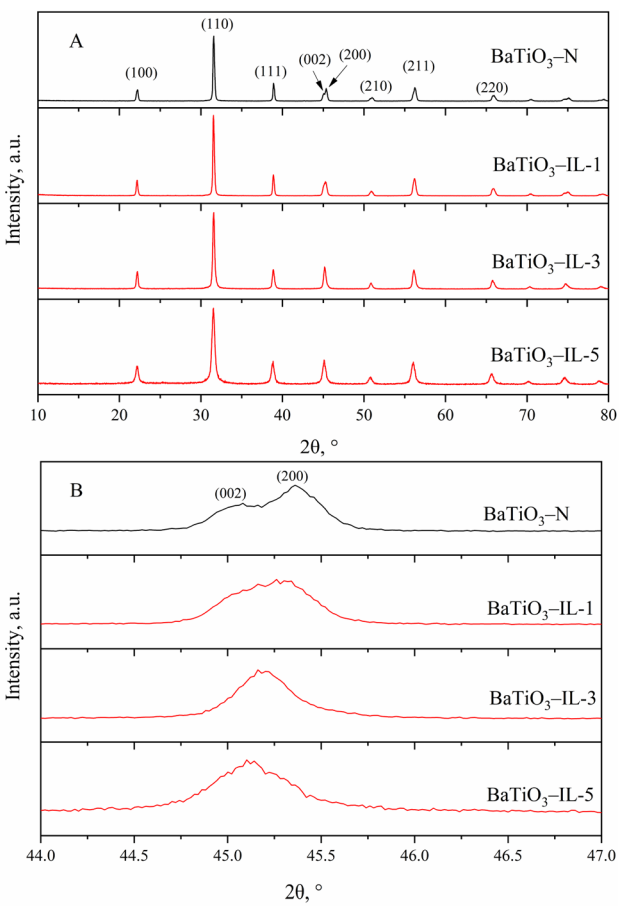

Fig. 1 XRD patterns of nano-$BaTiO_3$ ((A) full range; (B) in the 2θ range of 44.0–47.0°).

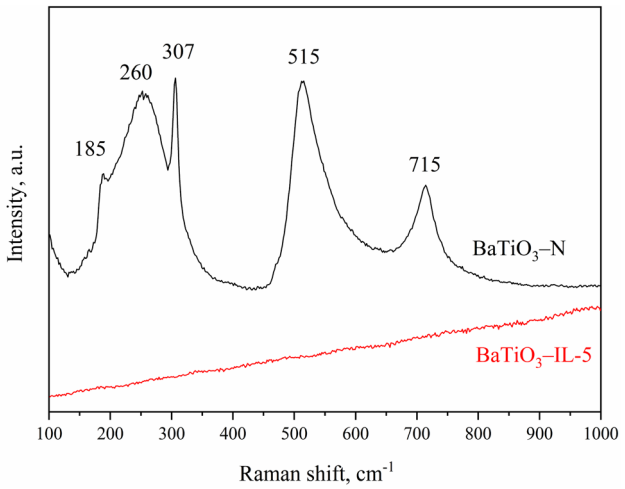

Fig. 2 Raman spectra of $BaTiO_3$-N and $BaTiO_3$-IL-5.

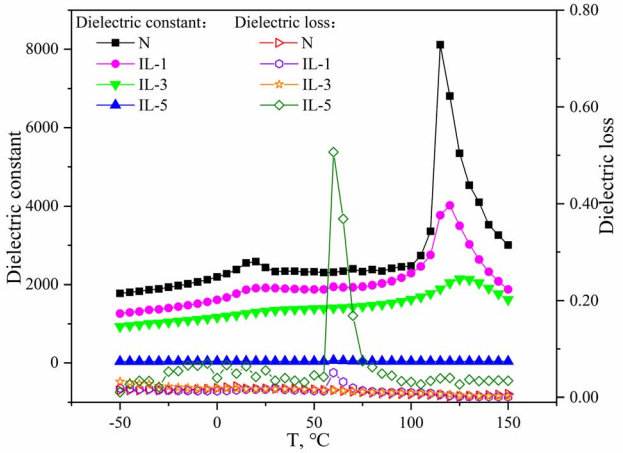

Fig. 4 Effect of ILs loadings on dielectric constant and dielectric loss of $BaTiO_3$ ceramics at different temperature.

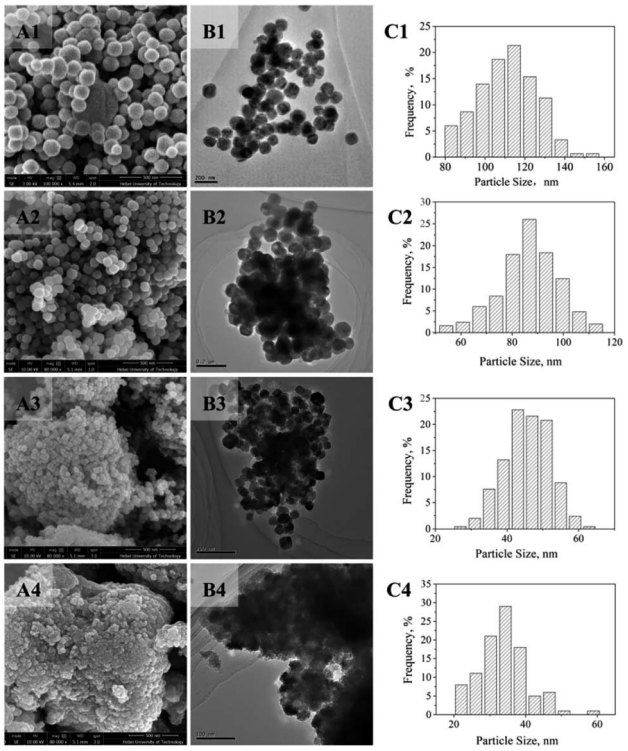

Fig. 3 SEM and TEM images, and particle size distributions, of nano-$BaTiO_3$. SEM: A1, $BaTiO_3$-N; A2, $BaTiO_3$-IL-1; A3, $BaTiO_3$-IL-3; A4, $BaTiO_3$-IL-5. TEM: B1, $BaTiO_3$-N; B2, $BaTiO_3$-IL-1; B3, $BaTiO_3$-IL-3; B4, $BaTiO_3$-IL-5. Size distributions: C1, $BaTiO_3$-N; C2, $BaTiO_3$-IL-1; C3, $BaTiO_3$-IL-3; C4, $BaTiO_3$-IL-5.

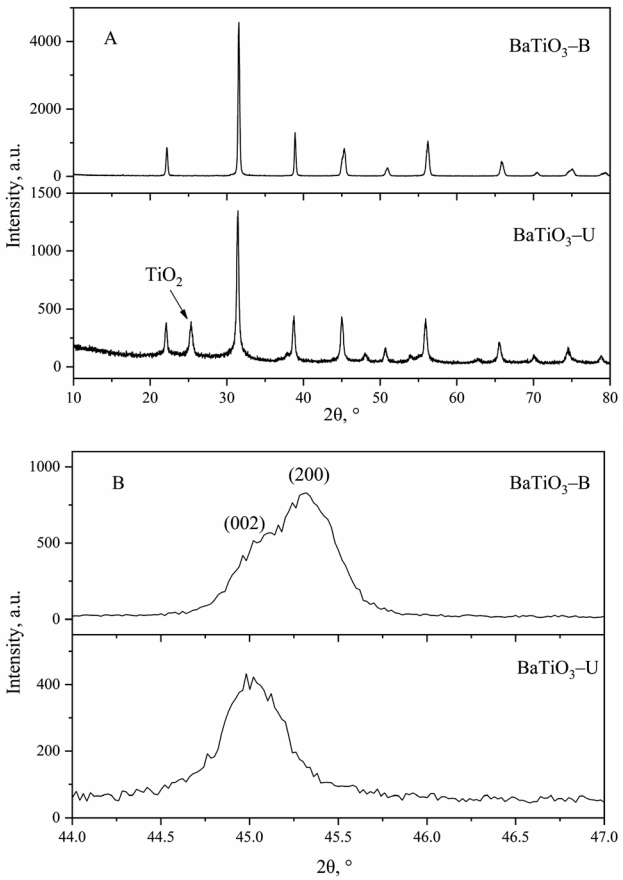

Fig. 5 XRD patterns of $BaTiO_3$-B and $BaTiO_3$-U ((A) full range; (B) in the 2θ range of 44.0–47.0°).

increasing quantity of ionic liquid,[40] which is not conducive to growth of $BaTiO_3$ microcrystals and thus also led to a gradual decrease in the particle size.

The dielectric properties of the aforementioned $BaTiO_3$ samples were evaluated at 1000 Hz after processing into ceramics; Fig. 4 shows the dielectric temperature curves. The dielectric constant of $BaTiO_3$-N with 95% tetragonal phase was *ca.* 2500 at room temperature and 8100 at the Curie temperature, and the dielectric loss was very small over the entire temperature range. With the addition of ionic liquid and the increase in the amount of ionic liquid, the dielectric constant of $BaTiO_3$-IL samples gradually decreased. The dielectric peak at

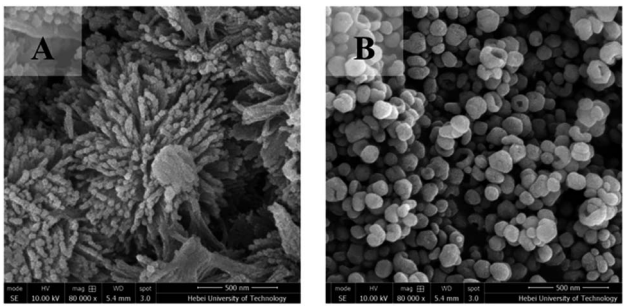

Fig. 6 SEM images of $BaTiO_3$-U (A) and $BaTiO_3$-B (B).

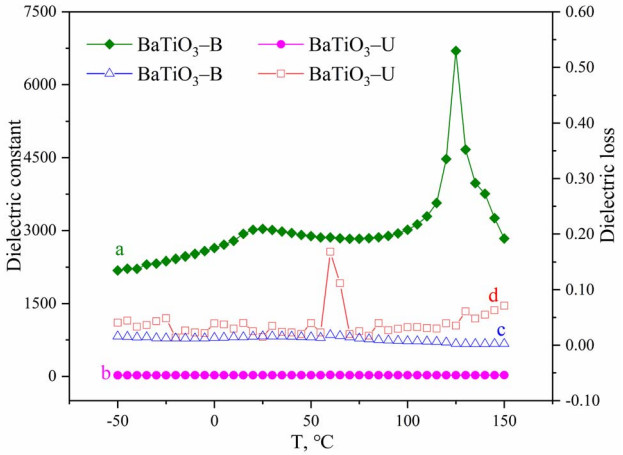

Fig. 7 Temperature-dependence of the dielectric constant and dielectric loss of $BaTiO_3$ ceramics with different morphologies.

Curie temperature gradually decreased and broadened, and the phenomenon of dielectric dispersion appeared, among which the dielectric loss of $BaTiO_3$-IL-1 and $BaTiO_3$-IL-3 did not change significantly compared with $BaTiO_3$-N samples. The dielectric constants of $BaTiO_3$-IL-1 and $BaTiO_3$-IL-3 at room temperature were 1900 and 1300, respectively, and at the Curie temperature were 4000 and 2000, respectively. When the amount of ionic liquid was increased to 5 g, the dielectric constant of $BaTiO_3$-IL-5 ceramic sample was very low, only about 40, and remained unchanged with the change of temperature. Its dielectric loss increases significantly. In accordance with these characterization results, the dielectric constant of $BaTiO_3$ ceramics increased with increasing tetragonal-phase content.

The densities of $BaTiO_3$-N and $BaTiO_3$-IL-5 ceramic samples were determined by Archimedes' method, which were 5.78 and 4.9 g cm^{-3}, respectively. According to the theoretical density of pure $BaTiO_3$ ceramics (6.08 g cm^{-3}), the relative densities of the two are calculated to be 95.1% and 80.6%, respectively. The low relative density of $BaTiO_3$-IL-5 ceramic sample is due to the use of a large amount of ionic liquid in the preparation process. Due to the decomposition of ionic liquid in the roasting process, the $BaTiO_3$-IL-5 ceramic sample is relatively loose. This is also one of the reasons for its poor dielectric properties. Similar results were obtained by Ashokkumar *et al.*[52] They prepared nano-sized $BaTiO_3$ with citric acid by hydrothermal method. The average grain size of $BaTiO_3$ ranges from 10–28 nm, and its dielectric constant is less than 50 when $T < 200$ °C, which increases with the increase of temperature.

Furthermore, the dielectric constants of the $BaTiO_3$ ceramics were also influenced by the particle size. $BaTiO_3$-IL-3 and $BaTiO_3$-IL-5 were both in the cubic phase, but the former exhibited a much larger dielectric constant than the latter because the particle size of $BaTiO_3$-IL-5 was only 34 nm. In accordance with Ruan *et al.*,[41] with decreasing grain size of $BaTiO_3$, the volume of the surface layer increased, resulting in incomplete crystallization and thus a smaller dielectric constant. In addition, there is a critical size of $BaTiO_3$. Upon reducing the grain size to a certain value, $BaTiO_3$ changes from tetragonal phase to cubic phase. Mandal *et al.*[37] suggested that the tetragonal phase content of nano-$BaTiO_3$ is negatively correlated with the grain size. Li *et al.*[42] reported that the critical size of $BaTiO_3$ was 56 nm, and the tetragonal phase was evident only when the grain size was >56 nm. Uchino *et al.*[43] obtained the critical size of $BaTiO_3$ to be *ca.* 44 nm by theoretical calculations. In the present study, the critical size could not be determined precisely because the grain size of the nano-$BaTiO_3$

Table 1 Comparison of $BaTiO_3$ prepared by different methods

Entry	Ti source	Ba source	Preparation method	D_p[a] (nm)	Dielectric constant	Ref.
1	TiO_2	$Ba(OH)_2 \cdot 8H_2O$	Hydrothermal	129	8100 (1 kHz)	This work
2	TiO_2	$Ba(OH)_2 \cdot 8H_2O$	Hydrothermal	86–34	4000–40 (1 kHz)	This work
3	TiO_2	$Ba(OH)_2$	Cold sintering	122	2332 (1 kHz)	49
4	$TiCl_4$	$BaCl_2 \cdot 2H_2O$	Hydrothermal	10–40	1106 (10 Hz)	50
5	$Ti(OC_4H_9)_4$	$Ba(NO_3)_2$	Oxalate co-precipitation assisted with microwave	30–50	7823.5 (1 kHz)	51
6	$Ti(i\text{-}OPr)_4$	$BaCl_2$	Hydrothermal	10–28	<50 (50 Hz–5 MHz)	52
7	TiO_2	$BaCO_3$	Two-step calcination	156	~12 800 (1 kHz)	53
8	$Ti[OCH(CH_3)_2]_4$	$BaCl_2$	Sol–gel	120–280	>120	54
9	TiO_2	$Ba(COOH)_2$	Sol–gel	287	117 (10 kHz, 25 °C)	55
10	TiO_2	$BaCO_3$	High energy ball milling	Submicron	2180 (20 Hz, Tc)	56

[a] Particle size.

was not continuous, but the results indicate that $BaTiO_3$ with a grain size of <46 nm was cubic phase.

3.2 Preparation of $BaTiO_3$ with various morphologies

$BaTiO_3$-U was prepared by the hydrothermal method with [Tmospmim]Cl as an additive, and $BaTiO_3$-B was prepared with PVP as a morphology control agent. Both were characterized (Fig. 5 and 6).

Based on the XRD pattern of $BaTiO_3$-B (Fig. 5), there was a split peak near 45°, indicating that it contained tetragonal phase. The axial rate c/a was 1.0081 and the tetragonal-phase content was *ca.* 90%. In contrast, the XRD pattern of $BaTiO_3$-U exhibited a single peak near 45°, indicating a cubic-phase structure. In addition, a diffraction peak of TiO_2 was evident in the XRD pattern of $BaTiO_3$-U,[48] which is the result of an incomplete hydrothermal process, indicating that adding PVP was not conducive to the reaction between TiO_2 and $Ba(OH)_2$.

Fig. 6A shows an SEM image of $BaTiO_3$-U. $BaTiO_3$-U exhibited a three-dimensional structure; which was a sea urchin-like structure consisting of small, one-dimensional, rod-like grains. The crystal plane energies of (100), (110), and (111) of $BaTiO_3$ are different, among which the crystal plane energy of (111) is the largest and the growth rate in this direction is also the fastest.[44] When there was no ionic liquid in the system, the morphology of the product was approximately spherical. Adding an ionic liquid to the solution can inhibit irregular growth of the particles by chelation with one of the crystal surfaces, and control the morphology as well as size of the product. In the present study, the quantity of ionic liquid used for preparing $BaTiO_3$-U was much larger than that for preparing $BaTiO_3$-IL, and its effect was more obvious. During formation of $BaTiO_3$, the ionic liquid adsorbs onto the (100) and (110) crystal planes through chelation, which reduces the crystal energy and decreased the growth rate, thus facilitating growth of $BaTiO_3$-U along the (111) crystal plane direction and formation of a one-dimensional rod structure. Moreover, the alkyl chains of ionic liquids can assemble and form micelles in water, and the resulting rod-like $BaTiO_3$ aggregates onto the surface of IL micelles in a manner that forms a sea urchin-like, three-dimensional structure.

Fig. 6B shows an SEM image of $BaTiO_3$-B. These particles were hollow and bowl-shaped, with an average size of 92 nm. Formation of hollow particles is usually based on the Ostwald ripening mechanism or the Kirkendall effect.[45,46] From a thermodynamic standpoint, during Ostwald maturation, larger particles are more stable than smaller particles, the latter of which exhibit a higher solubility and the ions that result from dissolution crystallize onto the surface of the larger particles, which further enlarges the particles. During diffusion of the ions, the smaller pores gradually increase and eventually form a hollow structure. The Kirkendall effect arises from the difference in ion diffusion rates at the interface. In a manner that compensates for the difference in diffusion rates during the internal diffusion of metal ions, there is vacancy diffusion, and the limited particle size and structural constraints lead to supersaturation of lattice vacancies, which initiates a concentration of over-generated interstitial spaces and eventually formation of hollow structures within the particles.

The effect of the $BaTiO_3$ morphology on the dielectric constant and loss was investigated; Fig. 7 shows the dielectric temperature curves. The room-temperature dielectric constant of $BaTiO_3$-B ceramics was 3000 and the dielectric constant at the Curie-temperature was 6700.

The density of the $BaTiO_3$-B ceramic sample was 5.36 g cm^{-3} and the relative density was calculated to be 88.2%. Compared with $BaTiO_3$-N, which exhibited a large dielectric constant as previously mentioned, $BaTiO_3$-B exhibited a relatively large room-temperature dielectric constant and a small Curie-temperature dielectric constant. Moreover, the dielectric loss of $BaTiO_3$-B ceramics was very small, similar to that of $BaTiO_3$-N. However, the dielectric constant of $BaTiO_3$-U ceramics was only about 25 and almost not changes with temperature, and the dielectric loss was significantly greater than that of $BaTiO_3$-B ceramics. As previously mentioned, the magnitude of the dielectric constant of $BaTiO_3$ is related to the quantity of tetragonal-phase content in the particle; $BaTiO_3$ with a high tetragonal-phase content exhibited a stronger electric field response. Based on the characterization results, $BaTiO_3$-U formed by agglomeration of small grains of cubic $BaTiO_3$, which exhibits no ferroelectricity; thus, its dielectric constant was low with large dielectric loss. In contrast, the content of the tetragonal phase in $BaTiO_3$-B was *ca.* 90%; thus, it exhibited a large dielectric constant and a small dielectric loss.

Table 1 lists some literature related to the preparation of $BaTiO_3$ in recent years, and compares them with the results of this work, including preparation methods, raw materials, particle size of the product, dielectric constant, *etc.* Compared with the existing research, this study is that the ionic liquid was added as a template in the hydrothermal synthesis of $BaTiO_3$, and the smaller size nanoparticles were prepared, with higher dielectric constant and lower dielectric loss. In addition, various morphologies of barium titanate were also prepared by adding ionic liquids or PVP, and its dielectric constant and other properties were investigated.

4. Conclusions

$BaTiO_3$ nanoparticles were prepared by the hydrothermal method with $Ba(OH)_2 \cdot 8H_2O$ and anatase TiO_2 as raw materials, and the ionic liquid of 1-(propyl-3-methoxysilyl)-3-methylimidazole chloride ([Tmospmim]Cl) as an additive. $BaTiO_3$-N nanoparticles prepared without an ionic liquid were spherical, with an average particle size of 129 nm, and the tetragonal content was *ca.* 95%. After adding the ionic liquid, the size of the $BaTiO_3$-IL decreased and the content of the tetragonal phase gradually decreased until all of the particles changed into the cubic phase. The dielectric property test results indicate that the dielectric constant of $BaTiO_3$-N ceramics was the highest, decreased with decreasing $BaTiO_3$ particle size, and the tetragonal-phase content decreased. Cubic-phase $BaTiO_3$ particles with a sea urchin morphology were prepared by changing the reaction conditions and the dielectric constant was low. In addition, bowl-shaped $BaTiO_3$-B

particles with an average size of 92 nm and a tetragonal-phase content of 90% were prepared with PVP instead of an ionic liquid. The dielectric constant of the prepared ceramics was 3000 at room temperature and 6700 at the Curie temperature.

Author contributions

Xinxiao Wu: data curation, formal analysis, writing-original draft. Weining Han: data curation, formal analysis. Hepan Zhao: writing review & editing. Zhimiao Wang: writing review, editing. Fang Li: conceptualization, methodology, visualization. Jing Li: supervision, funding acquisition. Wei Xue: supervision, conceptualization, methodology, writing-review & editing.

Conflicts of interest

The authors declare that they have no known competing financial interests or personal relationships that could have appeared to influence the work reported in this paper.

Acknowledgements

This work was supported by the National Natural Science Foundation of China (No. U21A20306, U20A20152), and Natural Science Foundation of Hebei Province (B2022202077). We thank Michael Scott Long, PhD, from Liwen Bianji (Edanz) (**www.liwenbianji.cn**) for editing the English text of a draft of this manuscript.

Notes and references

1 H. Qi, L. Fang, W. Xie, H. Zhou, Y. Wang and C. Peng, *J. Mater. Sci.: Mater. Electron.*, 2015, **26**, 8555–8562.
2 S. Y. Jun, S. H. Park, N. W. Baek, T. Y. Lee, S. Yoo, D. Jung and J. Y. Kim, *RSC Adv.*, 2022, **12**, 16412–16418.
3 H. Meng, Z. Chen, Z. Lu, X. Wang and X. Fu, *Process. Appl. Ceram.*, 2021, **15**, 179–183.
4 F. He, W. Ren, G. Liang, P. Shi, X. Wu and X. Chen, *Ceram. Int.*, 2013, **39**, S481–S485.
5 P. R. Bhunia, S. Gupta, A. Garg and R. K. Gupta, *J. Polym. Sci.*, 2022, **60**, 961–967.
6 G. L. Brennecka, J. F. Ihlefeld, J. P. Maria, B. A. Tuttle and P. G. Clem, *Int. J. Appl. Ceram. Technol.*, 2010, **93**, 3935–3954.
7 K. G. Baiju, A. Nagarajan, A. Sadasivam, D. Rajan and D. Kumaresan, *Asia-Pac. J. Chem. Eng.*, 2020, **15**, e2550.
8 D. H. Yoon and B. I. Lee, *J. Eur. Ceram. Soc.*, 2004, **24**, 739–752.
9 N. Sareecha, W. A. Shah, M. Anis-Ur-Rehman, M. L. Mirza and M. S. Awan, *Solid State Ionics*, 2017, **303**, 16–23.
10 C. Baek, J. E. Wang, S. Moon, C. H. Choi and D. K. Kim, *J. Am. Ceram. Soc.*, 2016, **99**, 3802–3808.
11 B. B. Jiang, J. Iocozzia, L. Zhao, H. F. Zhang, Y. W. Harn, Y. H. Chen and Z. Q. Lin, *Chem. Soc. Rev.*, 2019, **48**, 1194–1228.
12 L. R. Prado, N. S. D. Resende, R. S. Silva, S. M. S. Egues and G. R. Salazar-Banda, *Chem. Eng. Process.*, 2016, **103**, 12–20.
13 F. He, *Appl. Chem. Ind.*, 2010, **39**, 1754–1757.
14 M. Vijatović, J. Bobić and B. Stojanoić, History and challenges of barium titanate: Part I, *Sci. Sintering*, 2008, **40**, 155–165.
15 M. Vijatović, J. Bobić and B. Stojanoić, *Sci. Sintering*, 2008, **40**, 235–244.
16 N. J. Joshi, G. S. Grewal, V. Shrinet, A. Pratap and N. J. Buch, *Integr. Ferroelectr.*, 2010, **115**, 142–148.
17 H. Chen and Y. Chen, *Ind. Eng. Chem. Res.*, 2003, **42**, 473–483.
18 C. Liu, Y. Liu, C. An, H. Wang and X. Zhou, *Wujiyan Gongye*, 2012, **44**, 16–18.
19 Q. Ma, K. Mimura and K. Kato, *J. Alloys Compd.*, 2016, **655**, 71–78.
20 M. Inada, N. Enomoto, K. Hayashi, J. Hojo and S. Komarneni, *Ceram. Int.*, 2015, **41**, 5581–5587.
21 J. Li, S. Hietala and X. Tian, *ACS Nano*, 2015, **9**, 496–502.
22 Y. Zhu, L. Zhang, T. Natsuki, Y. Fu and Q. Ni, *ACS Appl. Mater. Interfaces*, 2012, **4**, 2101–2106.
23 R. A. Surmenev, R. V. Chernozem, A. G. Skirtach, A. S. Bekareva, L. A. Leonova, S. Mathur, Y. F. Ivanov and M. A. Surmeneva, *Ceram. Int.*, 2021, **47**, 8904–8914.
24 Y. Marfavi, R. Aliakbari, E. Kowsari, B. Sadeghi and S. Ramakrishna, in *Ionic Liquid-Based Technologies for Environmental Sustainability*, Elsevier, Amsterdam, The Netherlands, 2022, pp. 155–166.
25 J. Xia, Y. Ge, J. Di, L. Xu, S. Yin, Z. Chen, P. Liu and H. Li, *J. Colloid Interface Sci.*, 2016, **473**, 112–119.
26 C. Cruz and A. Ciach, *Molecules*, 2021, **26**, 3668.
27 Z. Chen, H. Ma, J. Xia, J. Zeng, J. Di, S. Yin, L. Xu and H. Li, *Ceram. Int.*, 2016, **42**, 8997–9003.
28 K. A. Prokop, M. Guzik, Y. Guyot, G. Boulon, M. Wilk-Kozubek, M. Sobczyk, A. V. Mudring and J. Cybińska, *Mater. Sci. Eng., B*, 2022, **275**, 115503.
29 J. Łuczak, M. Paszkiewicz, A. Krukowska, A. Malankowska and A. Zaleska-Medynska, *Adv. Colloid Interface Sci.*, 2016, **227**, 1–52.
30 X. Liu, J. Ma and W. Zheng, *Rev. Adv. Mater. Sci.*, 2011, **27**, 43–51.
31 Y. Zhou and M. Antonietti, *J. Am. Ceram. Soc.*, 2003, **125**, 14960–14961.
32 Y. Cao, S. Guo, C. Yu, J. Zhang and G. Li, *J. Mater. Chem. A*, 2020, **8**, 15767–15773.
33 M. Paszkiewicz, J. Luczak, W. Lisowski, P. Patyk and A. Zaleska-Medynska, *Appl. Catal., B*, 2016, **184**, 223–237.
34 T. Kim, W. Kim, S. Hong, J. Kim and K. Suh, *Angew. Chem. Int. Ed.*, 2009, **48**, 3806–3809.
35 Z. Z. Lazarević, N. Romčević, M. Vijatović, N. Paunović, M. Romčević, B. Stojanović and Z. Dohcević-Mitrović, *Acta Phys. Pol. A*, 2009, **115**, 808–810.
36 Y. Xie, Y. Shu, T. Hashimoto, Y. Tokano, A. Sasaki and T. Sato, *J. Eur. Ceram. Soc.*, 2010, **30**, 699–704.
37 T. K. Mandal, *Mater. Lett.*, 2007, **61**, 850–854.
38 S. R. K. Patel, P. Kumar, C. Prakash and D. K. Agrawal, *Ceram. Int.*, 2012, **38**, 1585–1589.
39 X. Duan, J. Ma, J. Lian and W. Zheng, *CrystEngComm*, 2014, **16**, 2550–2559.

40 Y. Ding, Y. Cao, Y. Guo, T. Sun, Y. Sun, Q. Ye, J. Li and C. Peng, *J. Chem. Eng. Data*, 2022, **67**, 1350–1357.
41 S. P. Ruan, W. Dong, F. Q. Wu, Y. W. Wang, Y. Tu and Z. H. Peng, *J. Phys. Chem.*, 2003, **42**, 17–20.
42 X. Li and W. H. Shih, *J. Am. Ceram. Soc.*, 1997, **80**, 2844–2852.
43 K. Uchino, E. Sadanaga and T. Hirose, *J. Am. Ceram. Soc.*, 1989, **72**, 1555–1558.
44 S. Adireddy, C. Lin, B. Cao, W. Zhou and G. Caruntu, *Chem. Mater.*, 2010, **22**, 1946–1948.
45 J. S. Cho, J. S. Park and Y. C. Kang, *Nano Res.*, 2017, **10**, 897–907.
46 Y. Liu, Q. Li, S. Gao and J. K. Shang, *J. Am. Ceram. Soc.*, 2013, **96**, 1421–1427.
47 P. Yu, W. Liu, P. Gao, T. Shao, S. Zhao, Z. Han, X. Gu, J. Zhang and Y. Wang, *J. Mater. Sci.: Mater. Electron.*, 2022, **33**, 10828–10840.
48 E. Song, H. K. Dong, E. J. Jeong, M. Choi, Y. Kim, H. J. Jung and M. Y. Choi, *Environ. Res.*, 2021, **202**, 111668.
49 J. P. Ma, X. M. Chen, W. Q. Ouyang, J. Wang, H. li and J. L. Fang, *Ceram. Int.*, 2018, **44**, 4436–4441.
50 K. G. Baiju, A. Nagarajan, A. M. G. Sadasivam, D. D. S. Rajan and D. Kumaresan, *Asia-Pac. J. Chem. Eng.*, 2020, **15**, e2550.
51 Q. Zhang, J. Chen and M. C. Che, *Ferroelectrics*, 2020, **566**, 30–41.
52 R. Ashokkumar, S. Gnanam, K. Senthil Kannan, M. Shanmugaprakash and S. Karthikeyan, *AIP Conference Proceedings*, AIP Publishing LLC, 2022, vol. 2446, p. 130006.
53 L. Zhang, J. Wen, Z. Zhang, J. Yang, H. Huang, Q. Hu, H. Zhuang and H. Yu, *Physica. B.*, 2019, **560**, 155–161.
54 W. Han, J. Kim and H. H. Park, *J. Korean Ceram. Soc.*, 2020, **57**, 213–219.
55 S. Islam, N. Khatun, M. S. Habib, S. F. U. Farhad, N. I. Tanvir, M. Aftab Ali Shaikh, S. Tabassum, D. Isiam, M. Sajjad Hossain and A. Siddika, *Heliyon*, 2022, **8**, e10529.
56 N. K. Verma, S. K. S. Patel, D. Kumar, C. B. Singh and A. K. Singh, *AIP Conference Proceedings*, AIP Publishing LLC, 2018, vol. 1953, p. 050075.